2D MODELING OF ELECTRO-HYDRODYNAMICS AND CHEMICAL KINETIC OF DRY AND HUMID AIR FLOW ACTIVATED BY CORONA DISCHARGES

O. EICHWALD[1*], J.P. SARRETTE[2], O. DUCASSE[1] AND M. YOUSFI[2]

[1]Université de Toulouse, UPS, INPT, LAPLACE (Laboratoire Plasma et Conversion d'Energie) Toulouse Cedex 9 F-31062, France
[2] CNRS, LAPLACE, Toulouse F-31062

*Corresponding author: eichwald@laplace.univ-tlse.fr

ABSTRACT

The present work is devoted to the 2D simulation of a point-to-plane Atmospheric Corona Discharge Reactor (ACDR) powered by a DC high voltage supply. The corona reactor is periodically crossed by thin mono filamentary streamers with a natural repetition frequency of some tens of kHz. The present study compares the results obtained in dry air and with a small amount of water vapour. The simulation involves the electro-dynamics, chemical kinetic and neutral gas hydrodynamic phenomena that influence the kinetics of the chemical species transformation. Each discharge stage lasts about one hundred of nanoseconds while the post-discharge stage occurring between two successive discharge phases lasts one hundred of microseconds. The ACDR is crossed by a lateral dry or humid air flow initially polluted with 400 ppm of NO.

1. INTRODUCTION

In the field of studies focused on Atmospheric Corona Discharge Reactor (ACDR) and as a complement to experimental investigations, the multi-dimensional simulation can be of great help in order to understand and identify the main phenomena and reactions that influence the complex processes involved in the pollution control of harmful species. However, several specificities considerably increase the simulation difficulties such as for instance (i) the strong non stationary problem of alternating discharge and post-discharge phases with a repetition rate of tens of kilohertz, (ii) the large differences in the space and time scales between the very fast processes occurring during the discharge phase inside the small micro-discharge filaments and the lower ones covering a larger ACDR volume during every post-discharge phase or (iii) the judicious choice of a minimal set of both chemical reactions and species the most representative of the experimental observations while preserving reasonable computing times, among others.

Due to these specific difficulties, the complexity of ACDR simulation was progressively enhanced from uniform chemical kinetics (see e.g. [1,2]) to simulation involving space non-uniformity in one or multi-dimensional domain and coupling one or several phenomena during the discharge and post-discharge phases (see e.g. [3-7]). Only recently some works were devoted to the 2D simulation of successive discharge/post-discharge phases in a multi-point-to-plan ACDR and for time scale extended up to some milliseconds in dry air [8].

In the present paper, we compare the solution of a 2D simulation of an ACDR composed of tree aligned points and crossed by a polluted dry or humid air flow. We follow in particular the spatio-temporal transformation of the NO pollutant until 3ms by coupling 30 successive discharge/post-discharge phases with a repetition rate of 10 kHz. The simulation involves the chemical kinetics and the energetic effects of the electrical discharges on the neutral gas dynamics, temperature and reactivity.

2. SIMULATION CONDITIONS

The design of the 2D ACDR is displayed in Fig.1. A grounded metallic plane is positioned at a distance d = 7 mm below the points and the inter-point distance e is constant and equal to 5 mm. A DC positive high voltage of 7.2 kV is applied on each point and an initial stationary lateral atmospheric gas flow of 5 $m.s^{-1}$ polluted by 400 ppm of NO crosses the ACDR from the right to the left hand side of the domain. The gas

is either dry (22% O_2, 78% N_2) or humid air (19.3% O_2, 77.4% N_2, 3.3%H_2O) at 300K. The discharge phases are characterized by the simultaneous propagation of 3 vertical mono-filament discharges located between each point and the grounded plane. The natural repetition frequency of the discharge phases is equal to 10 kHz. The characteristics of each micro-discharge are supposed similar to an individual DC mono-point-to-plane micro-discharge already studied elsewhere [9]. As a function of the simulation conditions (dry or humid air), the flow gas involves a choice of 7 or 14 neutral chemical species (N, O, H, OH, HO_2, H_2O_2, HNO_2, HNO_3, O_3, NO_2, NO, O_2, N_2, H_2O) reacting following 12 or 28 selected chemical reactions shown in table 1 with their corresponding reaction rates. The simulation domain is discretized in square structured meshes of 50µm×50µm size while it is assumed that micro-discharges have an effective diameter of 50µm which corresponds to the size of the chosen cells. Therefore, it is possible to inject in the cells located between each point and the plane, specific source terms of active species (N, O, H and OH) and energy both simulating the micro-discharge effects.

A complete description of the present model can be found in reference [8]. Briefly, the gas hydrodynamics is simulated using the commercial ANSYS Fluent CFD software while the discharge effects are simulated as thermal and primary radical source terms that are applied periodically inside thin filamentary volumes located below each point. The source terms are applied every 0.1 ms during 150 ns, which corresponds to a typical DC corona discharge frequency (~10 kHz) and duration. The amplitude and spatial profile of each thermal and kinetic source term are calculated from a more global discharge model [9].

3. RESULTS AND DISCUSSIONS

Figures 1 to 4 show the obtained results for NO, O_3 and OH after 1, 2 and 3 ms, which corresponds to 10, 20 and 30 discharge/post-discharge cycles. The results are collected at the end of the post-discharge phase just before a new discharge injection. Figs 1 and 2 clearly show that the spatial regions where the NO density decreases correspond to the regions where the concentration of O_3 is the highest. This is mainly due to reaction (7) which transforms NO into NO_2 via O_3. It is noteworthy that the 3 body reactions (5) and (6) that also oxidize NO are efficient only during a very short time (~0.2 µs) and take place only in each small discharge volumes where the primary radicals O are created by direct dissociation of O_2 via electron impacts. The direct correlation between NO loss and O_3 concentration is also visible in Fig.4 showing the time evolution of the mean concentration integrated over the whole ACDR volume.

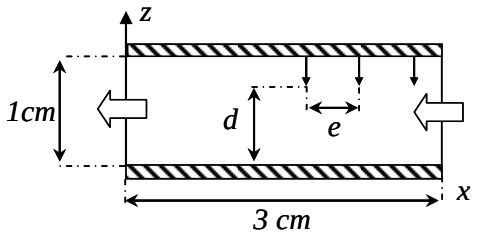

Fig. 1: Design of the 2D simulated multi-point-to-plane ACDR. An initial laminar flow of 5 m.s^{-1} polluted by 400 ppm of NO crosses the gap from the right hand side towards the left hand side of the reactor.

Table 1: Chemical kinetics reaction scheme used for dry (reactions 1 to 12) and humid (all reactions) air. The values of the coefficient reaction k expressed in m^3.s^{-1} or m^6.s^{-1} are given at 300K.

	Reactions	*k* (300K)
1	$N + O_2 \rightarrow NO + O$	$9.59\ 10^{-17}$
2	$N + NO \rightarrow N_2 + O$	$3.25\ 10^{-11}$
3	$O + N + O_2 \rightarrow NO + O_2$	$1.04\ 10^{-32}$
4	$O + N + N_2 \rightarrow NO + N_2$	$1.04\ 10^{-32}$
5	$O + NO + O_2 \rightarrow NO_2 + O_2$	$7.07\ 10^{-32}$
6	$O + NO + N_2 \rightarrow NO_2 + N_2$	$7.07\ 10^{-32}$
7	$O_3 + NO \rightarrow O_2 + NO_2$	$1.87\ 10^{-14}$
8	$O + NO_2 \rightarrow NO + O_2$	$1.02\ 10^{-11}$
9	$N + N + N_2 \rightarrow N_2 + N_2$	$4.39\ 10^{-33}$
10	$O + O_2 + O_2 \rightarrow O_3 + O_2$	$6.02\ 10^{-34}$
11	$O + O_2 + N_2 \rightarrow O_3 + N_2$	$6.02\ 10^{-34}$
12	$O_3 + N \rightarrow NO + O_2$	$1.00\ 10^{-16}$
13	$O_3 + H \rightarrow OH + O_2$	$2.82\ 10^{-11}$
14	$O_3 + OH \rightarrow HO_2 + O_2$	$7.41\ 10^{-14}$
15	$OH + OH + N_2 \rightarrow H_2O_2 + N_2$	$7.20\ 10^{-33}$
16	$OH + OH \rightarrow H_2O_2$	$2.61\ 10^{-11}$
17	$OH + OH \rightarrow H_2O + O$	$3.99\ 10^{-06}$
18	$OH + HO_2 \rightarrow H_2O + O_2$	$1.10\ 10^{-10}$
19	$OH + O \rightarrow O_2 + H$	$3.47\ 10^{-11}$
20	$OH + N \rightarrow NO + H$	$5.05\ 10^{-11}$
21	$OH + NO + N_2 \rightarrow HNO_2 + N_2$	$8.41\ 10^{-37}$
22	$OH + NO + O_2 \rightarrow HNO_2 + O_2$	$8.41\ 10^{-37}$
23	$OH + NO_2 + N_2 \rightarrow HNO3 + N_2$	$1.70\ 10^{-37}$
24	$OH + NO_2 + O_2 \rightarrow HNO3 + O_2$	$1.44\ 10^{-37}$
25	$HO_2 + NO \rightarrow OH + NO_2$	$1.10\ 10^{-11}$
26	$HO_2 + NO_2 \rightarrow HNO_2 + O_2$	$1.20\ 10^{-13}$
27	$H + HO_2 \rightarrow OH + OH$	$7.17\ 10^{-11}$
28	$H + O_2 + N_2 \rightarrow HO_2 + N_2$	$1.98\ 10^{-34}$

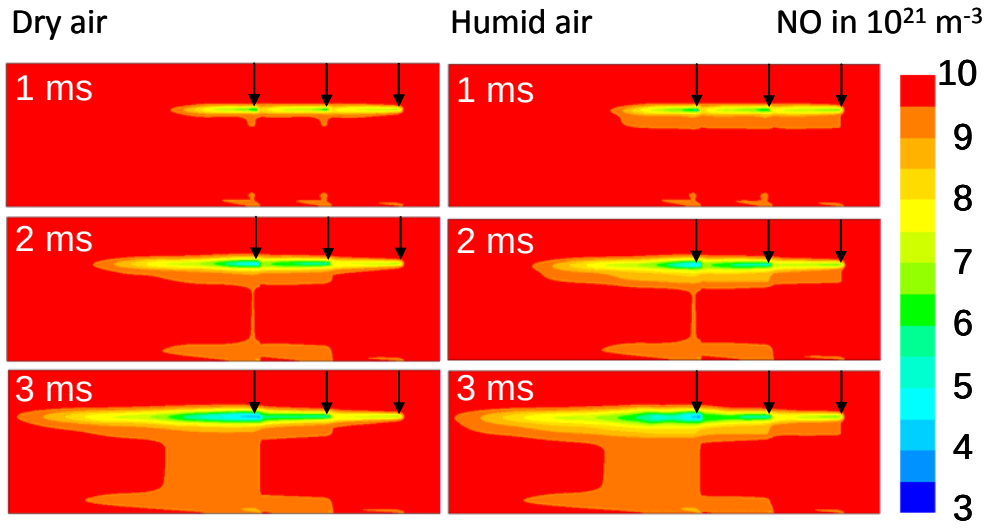

Fig.1 : Spatio-temporal evolution of the NO density (10^{21} m^{-3}) in the case of dry and humid air

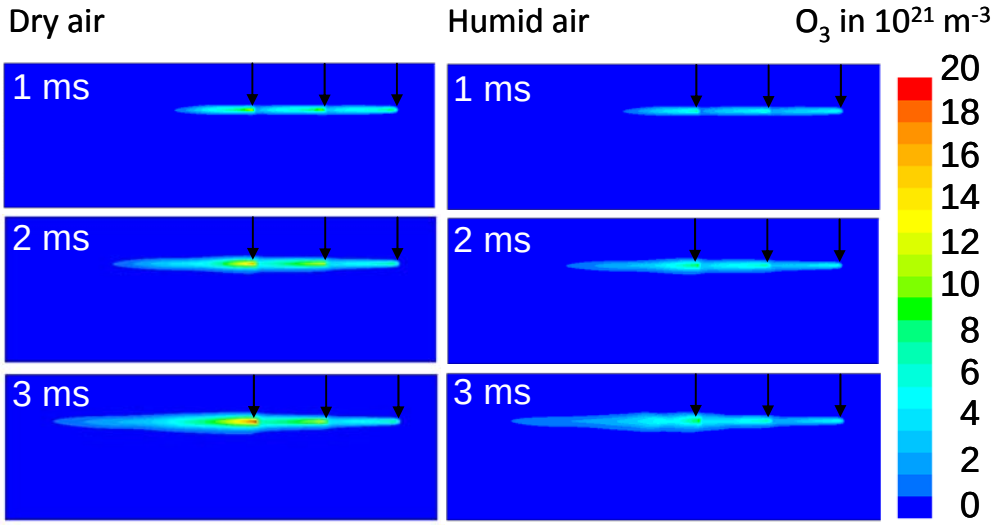

Fig. 2: Spatio-temporal evolution of the O_3 density (10^{21} m^{-3}) in the case of dry and humid air.

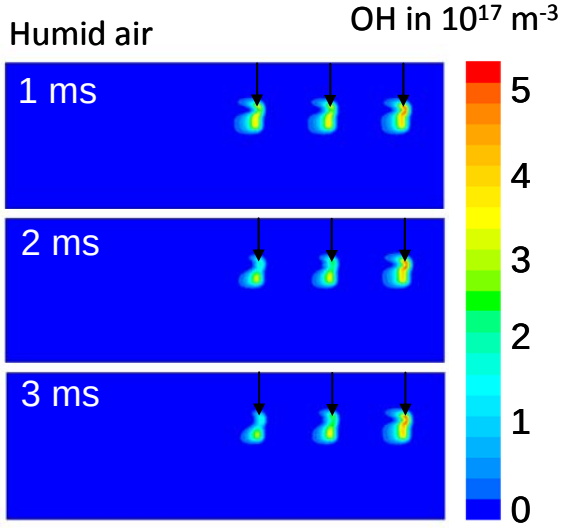

Fig. 3: Spatio-temporal evolution of the OH density (10^{17} m^{-3})in humid air.

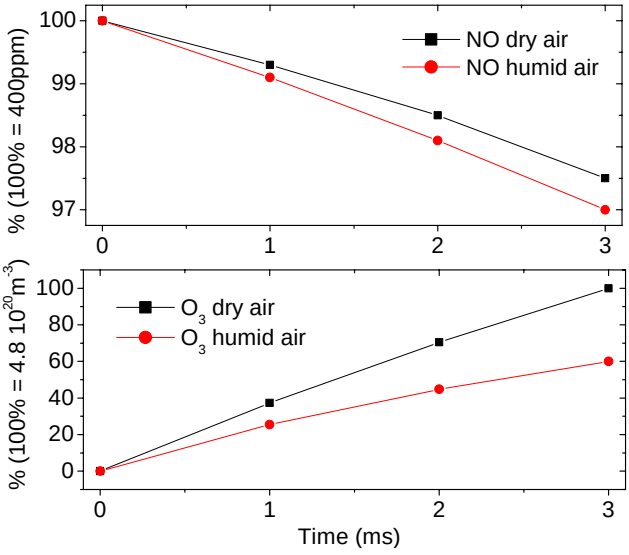

Fig.4 : Relative mean concentrations of NO and O_3 inside the whole ACDR volume as a function of time.

However, in humid air, the NO oxidation is slightly more efficient than in dry air even if the O_3 concentration is lowest. In fact, in humid air, the O_3 concentration is lowest because just after the discharge phase, reactions (13) and (14) involving the H and OH primary radicals consume a part of the ozone species formed during each discharge phase by reactions (10) and (11). Nevertheless, the NO oxidation remains highest in humid air due to the presence of the OH and HO_2 radicals that permits the NO oxidation through reactions (21), (22) and (25). Indeed, in humid air, and just after each discharge phase, the reaction (14) transforms locally O_3 into HO_2, the latter oxidizing rapidly NO through reaction (25). After each discharge phase, the OH radicals are transported in the lateral gas flow and interact with NO pollutant and the main gas molecules to progressively form HNO_2 via reactions (21) and (22). Therefore, at the end of each post-discharge phase and just before a new discharge phase, the OH radical does not show the lateral plume concentration, as observed for the NO or the O_3 cases (compare the concentration profile displayed in Fig. 3 with those in Figs. 1 and 2). Nevertheless, around the point, the OH concentration fall down from more than $10^{20}m^{-3}$ at the end of a discharge phase to about $10^{17}m^{-3}$ at the end of a post-discharge phase.

4. CONCLUSION

The present preliminary results have shown that contrarily to a more classical 0D model assuming a volume average reactivity, the reactions involving the primary radicals (such as OH or O) affect the NO evolution only in the surrounding of the small volume of the filamentary discharges while the reactions involving the secondary species (such as ozone) are mainly efficient in larger regions depending on the flow gas velocity. After 30 discharge/post-discharge cycles, the NO destruction in humid air is slightly more efficient than in dry air because of the oxidation reactions through radicals OH and HO_2.

ACKNOWLEDGMENT

This work was performed using HPC resources from CALMIP (Grant 2011-[P1053]) [29].

REFERENCES

[1] I. A. Kossyi, A. Yu Kostinsky, A. A. Matveyev & V. P. Silakov, “Kinetic scheme of the non equilibrium discharge in nitrogen-oxygen mixtures”, Plasma Sources Sciences and Technologies, vol. 1, pp. 207-220, 1992.

[2] I. Orlandini and U. Riedel, “Chemical kinetics of NO removal by pulsed corona discharges”, Journal of Physics D: Applied Physics, vol. 33, pp. 2467–2474, 2000.

[3] A. C. Gentile and M. J. Kushner, "Microstreamer dynamics during plasma remediation of NO using atmospheric pressure dielectric barrier discharges”, Journal of Applied Physics, vol. 79, pp. 3877-3885, 1996

[4] O. Eichwald, M. Yousfi, A. Hennad, and M. D. Benabdessadok, “Coupling of chemical kinetics, gas dynamics, and charged particle kinetics models for the analysis of NO reduction from flue gases”, Journal of Applied Physics, vol. 82, pp. 4781-4794, 1997.

[5] O. Eichwald, N. A. Guntoro, M. Yousfi, and M. Benhenni, “Chemical kinetics with electrical and gas dynamics modelization for NOx removal in an air corona discharge”, Journal of Physics D: Applied Physics, vol. 35, pp. 439-450, 2002.

[6] R. Dorai and M. J. Kushner, “Consequences of unburned hydrocarbons on microstreamer dynamics and chemistry during plasma remediation of NOx using dielectric barrier discharges”, Journal of Physics D: Applied Physics, vol. 36, pp. 1075–1083, 2003.

[7] E. Marode, D. Djermoune, P. Dessante, C. Deniset, P. Ségur, F. Bastien, A. Bourdon and C. Laux “Physics and applications of atmospheric non-thermal air plasma with reference to environment”, Plasma Phys. Control. Fusion, 51 124002 2009

[8] Meziane M., Eichwald O., Sarrette J. P., Ducasse O., Yousfi M., and Marchal F., “Electro-hydrodynamics and kinetic modelling of polluted air flow activated by multi-tip-to-plane corona discharge”, Journal of Applied Physics 113, 153302 (10pp) 2013

[9] O. Eichwald, O. Ducasse, , D. Dubois, A. Abahazem, N. Merbahi, M. Benhenni, and M. Yousfi, “Experimental analysis and modelling of positive streamer in air: towards an estimation of O and N radical production”, Journal of Physics D: Applied Physics, vol. 41, 234002 (11pp), 2008.

[10] www.calmip.cict.fr/spip/spip.php?rubrique90” for more information about the High Power Computer “Hyperion” used for calculation presented in this paper.